Seismic Attributes and the Road Ahead

By Kurt J. Marfurt, The University of Oklahoma - ***Part 1 of 2***

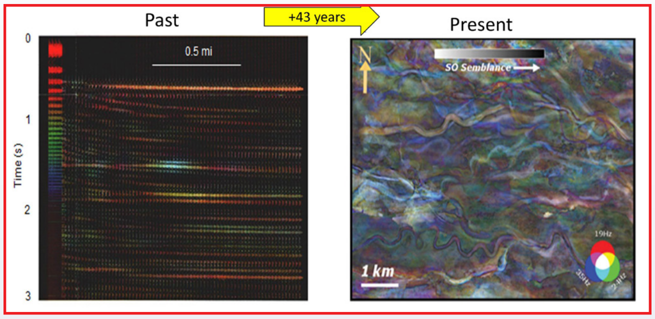

Figure 1: The advancement in spectral decomposition (and color display!) from (left) its introduction by Balch (1971) of a suite of band-pass filtered versions of the seismic data to more modern continuous wavelet transform, matching pursuit, and constrained least-squares spectral analysis in today's commercial software. (Right) McArdle et al. (2014) show 19 Hz, 24 Hz, and 35 Hz matching pursuit spectral components plotted against RGB co-rendered with structure-oriented coherence using a semblance algorithm plotted against black using opacity. The use of RGB and opacity provides 32-bit color.

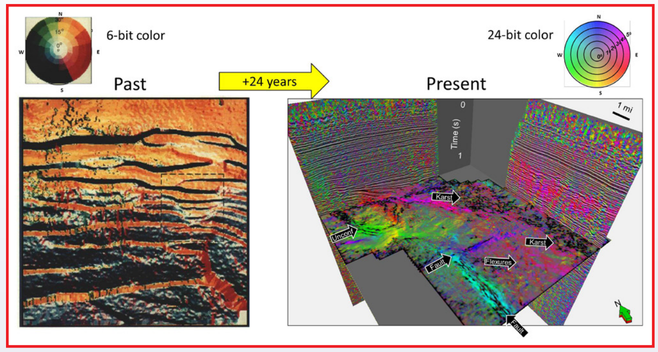

Figure 2: The advancement in geometric attributes (and again, color display!) from (left) the introduction co-rendered dip-magnitude and dip-azimuth horizon computations by Rijks and Jauffred (1991) using a 6-bit 2D colorbar (approaching 64 colors) to (right) a modern commercial implementation of volumetric dip magnitude, dip azimuth, and coherence display by Marfurt (2015) simulating an HLS color bar through the use of opacity, thereby resulting in 8-bits for each attribute or 24-bit color (some 20 million colors).

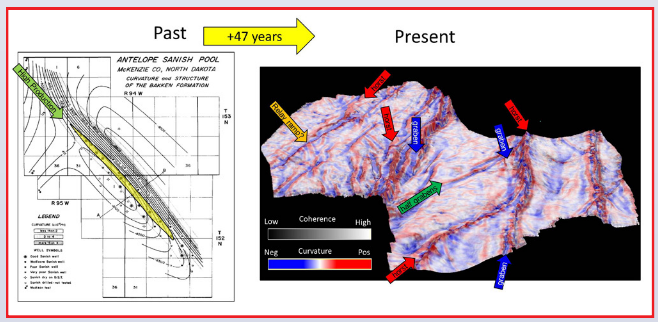

Figure 3: The advancement in geometric attributes that measure strain, and depending on the lithology, may be correlated to natural fractures. (Left) Murray (1968) image of perhaps the first examples of horizon based curvature computed from well tops showing higher production over a Bakken Shale reservoir. (AAPG©1968, reprinted by permission of the AAPG whose permission is required for further use). (Right) A modern implementation of volumetric curvature computed from 3D seismic data showing horsts, grabens, and possible relay ramps of a deformed carbonate in the Western Canadian Sedimentary Basin (after Chopra and Marfurt, 2015).

Summary

Seismic attributes were introduced to seismic interpretation four decades ago and now form a part of almost every seismic interpretation workflow. I predict a future of increasing interactive computer-interpreter linkage into areas that we now consider seismic processing. I also predict an increase in the use of cluster analysis and statistical correlation to completion processes and production data in resource plays.

The Past

Seismic attributes were first introduced to the geophysical community almost 43 years ago when Balch (1971) proposed co-rendering three different bandpass-filtered versions of the seismic data (what we would call today "spectral components") against red, green and blue (***Figure 1a***). Such analysis 43 years later is almost routine, with spectral decomposition being routinely used to map channels and other stratigraphic features at the limits of seismic resolution (***Figure 1b***). Subsequent developments by Taner et al. (1979) of instantaneous attributes generated initial excitement, but truly came into common usage with the advent of 3D interpretation workstations where Bahorich and van Bemmel (1994) showed that one could make maps of these attributes along interpreter-generated surfaces.

The introduction and adoption of 3D seismic data was followed by the development of 3D "geometric attributes" such as dip magnitude/dip azimuth (Rijks and Jauffred, 1991) (***Figure 2a***) , coherence (Bahorich and Farmer, 1995), and curvature (Roberts, 2001). In 2015 "attributes" - be they simple RMS maps or sophisticated waveform classifications - have become an integral part

Technical Article continued on page 12.

Technical Article continued from page 11.

of almost all interpretation workflows. While attributes such as coherence and RMS amplitude provide valuable images by themselves, many attributes form natural components of a vector, such as dip magnitude and dip azimuth which through the use of 24 bit color in turn can be modulated by a third attribute, such as coherence (***Figure 2b***). Attributes are best used when coupled through a geologic model, such as the early observation by Murray (1968) that flexures measured through well tops and 3D seismic data can be correlated to open fractures and thus better production (***Figure 3a***). Attributes such as curvature allow us to see features such as relay ramps that might otherwise be overlooked in a more conventional seismic interpretation workflow (***Figure 3b***).

Spectral decomposition and coherence (***Figure 1b***) provide a means of mapping the preserved components of a depositional system through geologic time, where skilled interpreters map point bars, fans, levees, and other architectural elements that may be more sand- vs. shale prone. Heritier et al. (1979) recognized that sand-rich components often compact less than shale-rich components, resulting in topographic features that can be seen on 2D sections (***Figure 4a***). 36 years later, we can map the same features and infer lithology volumetrically (***Figure 4b***). Stratigraphers use reflector truncations as an aid in mapping sequence boundaries and depositional packages. Masaferro et al. (2003) showed how one could flatten a seismic volume on a reference surface and then use volumetric dip and azimuth to map the angle and azimuth of a carbonate shoal facies (***Figure 5a***). 12 years later, we can do the same computations volumetrically without the need to first flatten (***Figure 5b***).

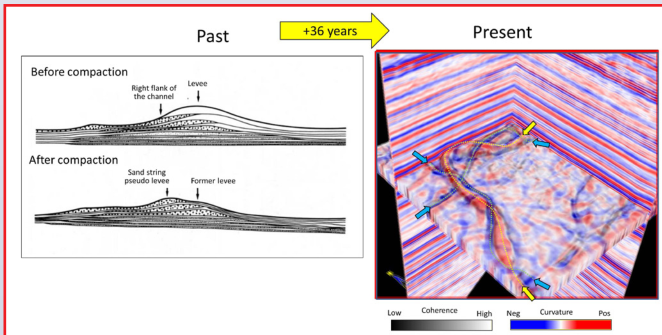

Figure 4: (Left) Heritier et al.'s (1979) model of differential compaction over a channel levee complex in the North Sea seen on 2D seismic data. (AAPG©1979, reprinted by permission of the AAPG whose permission is required for further use). (Right) Differential compaction seen on volumetric curvature co-rendered with coherence computed from a 3D seismic volume acquired in the Western Canadian Sedimentary Basin. Channels that appear as blue (negative curvature) are synclinal, have undergone more compaction than the surrounding flood plane, are probably filled with shale. In contrast, channels that appear as red (positive curvature) are anticlinal, have undergone less compaction than the flood plain, and possibly filled with sand. (After Chopra and Marfurt, 2015).

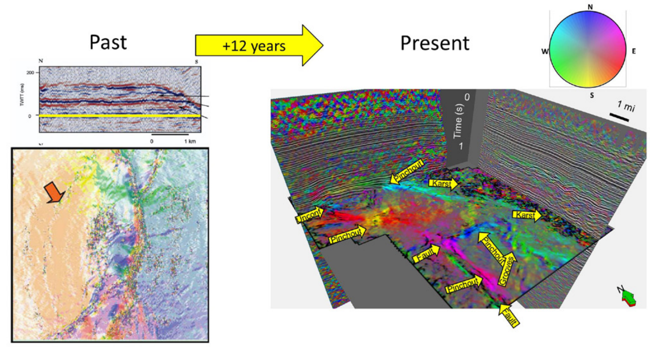

Figure 5: (Left) Perhaps the first example of example of computing the magnitude and azimuth of reflector convergence by Masaferro et al.'s (2003) for a Middle East carbonate shoal. The data were first flattened on a slightly deeper reference horizon. The volumetric dip and azimuth were then computed from the flattened data. The colors show the azimuth of convergence (pinch out) while the saturation of the color shows its magnitude, with white indicating parallel reflectors. (Right) A more recent volumetric implementation of reflector convergence where the convergence is computed by taking the curl of the vector dip (after Marfurt, 2015).

We have also made tremendous advancement in the development of "attributes" that are tightly connected to rock properties. Lindseth (1979) developed one of the first P-wave impedance algorithms, which was used to extend measurements made in wells to a grid of 2D seismic lines (***Figure 6a***). 35 years later, prestack P- and S-impedance inversion is done on desktop computers using commercial software (***Figure 6b***), while prestack geostatistical inversions providing probabilistic estimates of lithology, porosity, and fluid product are offered by several service companies.

Cluster analysis of multiple attributes started with k-means in the 1970s, but the more promising commercial products were correlation-based, either by computing a similarity index of the average waveform (suite of samples) about a producing well to all other traces on that horizon, or by generalizing the concept to mapping the similarity of a suite of attributes to all other traces on the that horizon (***Figure 7a***). A more recent innovation is to map not a vector of attributes at one voxel but rather a vector of attributes (in Stephen's 2011 example, of inverted Poisson's ratio) that represents the vertical stacking pattern of lithologies critical to effective completion processes (***Figure 7b***).

Technical Article continued on page 13.

Technical Article continued from page 12.

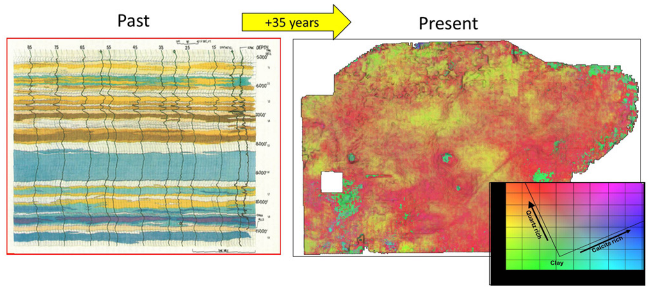

Figure 6: The advancement in impedance inversion from (left) Lindseth's (1979) 2D band-limited post stack P-wave impedance to (right) a modern implementation of 3D prestack simultaneous inversion for P- and S-wave impedances (after Perez-Altamar and Marfurt, 2014), which in this case has been color plotted against a mineralogy template computed from electron capture spectroscopy, P-wave sonic, S-wave sonic, and density logs.

The Present

Today, interpreters work with ever-larger data volumes with increased vertical and lateral resolution, providing images of subtle features that have not been previously documented in the published literature. The work by Bueno et al. (2014) is representative of this effort, where they link attribute images and modern clustering technology, to a modern analogue to develop an integrated geologic model (***Figure 8***).

Some areas are more challenging. While the "visual" correlation between curvature and fractures reported by Murray (1968) (***Figure 2b***) is commonly encountered, the numerical correlation has been more difficult to make. Clay model studies such as that shown in ***Figure 9*** validate an underlying principle learned (and forgotten by this author) in structural geology. Small deformation (small values of curvature) result in elastic deformation, with no fractures. Further deformation (increasing curvature) results in a monotonically increasing number of fractures until the distance between fractures approaches the thickness of the layer, called the saturation point. Beyond this limit, subsequent deformation is accommodated by movement along these fractures, which are now called faults. Examining ***Figure 9b***, we note the relationship between curvature is non-linear, where both the initialization and saturation point of fracturing are defined by thresholds. Given image log or other fracture measurements, at least one service provider has made progress in establishing these nonlinear relationships.

The relationship between faults and fractures depends on not only layer thickness, but also the lithology and the type of fault and resulting perturbation of the stress field. The work by Bourne et al. (2000) (***Figure 10***) is often cited by geoscientists and engineers working resource plays, many of which are cut by strike-slip faults. In their outcrop study (***Figure 10b***), they find that fractures on the north side are nearly perpendicular while those on the south side of the fault are nearly parallel to an intervening strike-slip fault. Recent work by Guo et al. (2014) asks more questions than it answers. ***Figure 11a*** shows a curvature image through two seismic surveys, where the survey to the NW was acquired after 400 wells were drilled and hydraulically

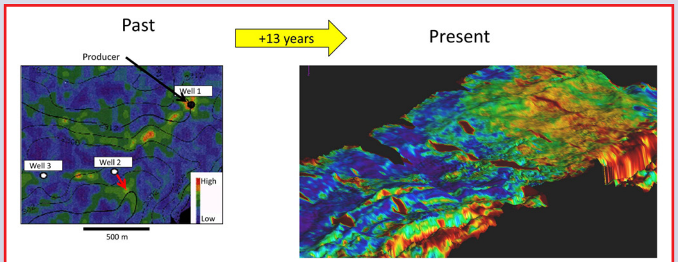

Figure 7: An early example of clustering by Michelena (1998) computing a similarity index (similar to crosscorrelation) between attribute vectors along a horizon. Well 1 was a producer while well 2 was a dry hole. The location of well 3 was to a new location that was structurally high and had an attribute response similar to the well 1 and also produced. (Right) A more recent clustering application using a self-organizing map. Rather than compute similar waveforms, Stephens (2011) computed similar vertical stacking patterns within an Eagle Ford Shale zone using prestack inversion estimates of Poisson's ratio at each trace location.

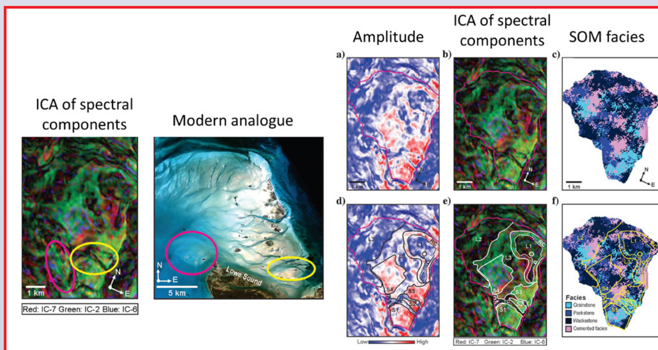

Figure 8: (Left) Composite RGB image independent component analysis of spectral decomposition of a reservoir offshore Brazil and a satellite image of a modern Bahama analogue. Yellow ellipses show channels and pink ellipses show flood tidal delta lobes in the seismic attributes and in the satellite image. (Right) Further analysis using modern analogues coupled with self-organizing map analysis of the ICA components and other attributes such as sweetness and coherence allows a prediction of the four most important facies. (After Bueno et al., 2014).

Technical Article continued on page 14.

Technical Article continued from page 13.

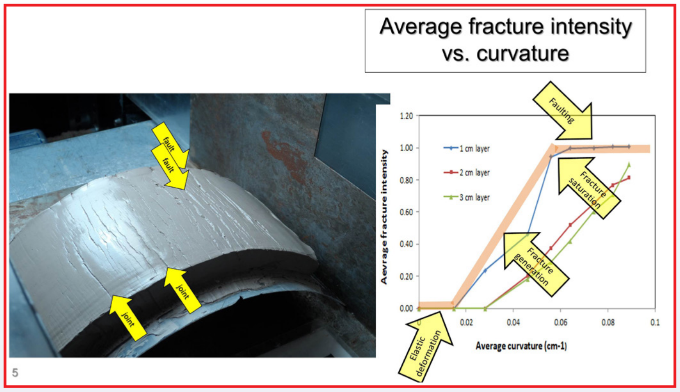

Figure 9: (Left) A simple fold using clay upon an plexiglas sheet. Model was slowly deformed over a period of several hours. (Right) Graph of average fracture intensity vs. average curvature in 1 cm, 2 cm, and 3 cm experiments. Note this behavior is NOT linear. Determining these kind of relations where there are thresholds involved is one of the challenges in the future. (After White, 2013).

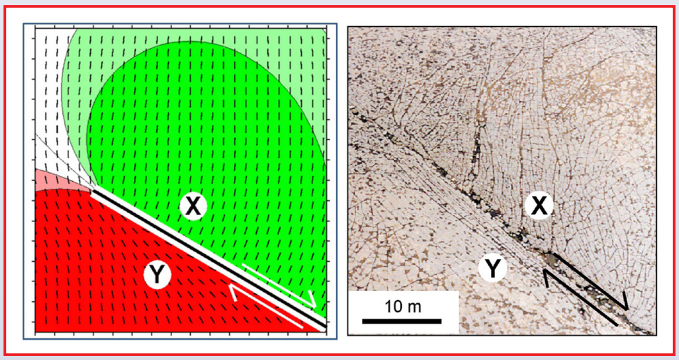

Figure 10: Work by Bourne et al. (2000) correlating the (left) predicted stress about a strike-slip fault tip to (right) the natural fractures seen in an outcrop in Wales. Note that at point X the fractures are at a high angle to the fault while at point they are nearly parallel to the fault.

fractured. The smaller survey to the SE was acquired prior to hydraulic fracturing. Not surprisingly, hydraulic fracturing does not affect the structure of the underlying geology, with similar SW-NE trending strike-slip faults going through both surveys. In contrast, the azimuthal anisotropy response shown in ***Figure 11b*** is quite different. In the SE survey, the intensity (brightness of the colors) of the azimuthal anisotropy is quite large, and shows similar angular relationships to the strike slip faults as seen in ***Figure 10b*** – parallel on one side, and perpendicular on the other. In the survey acquired after hydraulic fracturing to the NW, the anisotropy intensity is both muted, and the azimuthal relationship less pronounced. Our hypothesis is that hydraulic fracturing reduces azimuthal anisotropy, either by rubblizing the reservoir or by inducing orthogonal fractures making the reservoir behave as an orthotropic

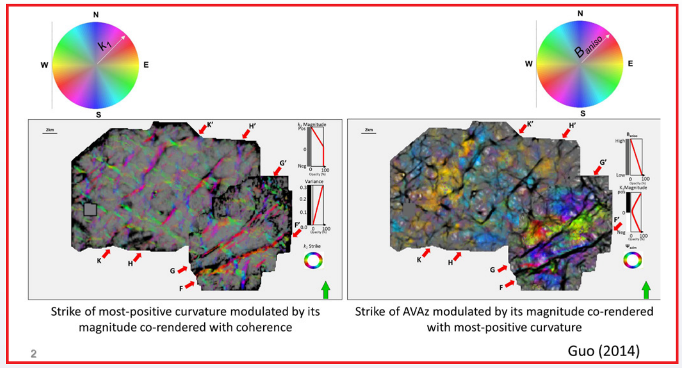

Figure 11: Phantom horizon slices through two adjacent surveys 20 ms above the base Barnett Shale through (left) the strike of most-positive curvature modulated by its magnitude co-rendered with coherence and (right) the strike of AVAz modulated by its magnitude co-rendered with most-positive curvature. Faults FF' and GG' are strike-slip faults associated with the Mineral Wells Fault of the Fort Worth Basin. In the survey to the SE, there is a strong correlation between the ridges seen in positive curvature and the magnitude and direction of the AVAz anomalies, interpreted to be proportional to the maximum stress direction. The survey to the NW was acquired after hydraulically fracturing the shale by more than 400 wells and shows reduced AVAz anomalies and reduced correlation to the structural deformation.

media. Without access to a true time-lapse seismic survey, the impact of hydraulic fracturing on surface seismic measures remains largely unknown.

As an associate editor for Geophysics (and now Interpretation) for almost 30 years, I often come across novel ways of examining seismic data that seem to violate our seismic imaging principles. One such paper was by Gao (2012) who used an analogue of light scattering from a compact disk (***Figure 12b***) to explain changes in reflectivity with azimuth and angle. The scattering of energy from a rugose surface will change with frequency. Furthermore, if the rugosity is organized, such as by a suite of fractures, the spectra will change with frequency as well. Such features fall well below the resolution limits of a migrated Fresnel zone, but that does not mean that we cannot detect rather than resolve them (***Figure 12a***).

Somewhat related to the concept of accurate imaging is the recent work on diffraction imaging. Original work by Kozlov (2004) suggested throwing away the information content of the first one or two Fresnel zones. In theory, an accurate migration algorithm should place the diffractions where they belong – at the ends of broken reflectors. In practice, our velocities are inaccurate, and the specular reflectors are an order of magnitude stronger than the diffractions. This would be acceptable except in many plays, mapping natural (and one day, induced) fractures is critical to successful completion strategies. The workflow is thus to

Technical Article continued on page 15.

Technical Article continued from page 14.

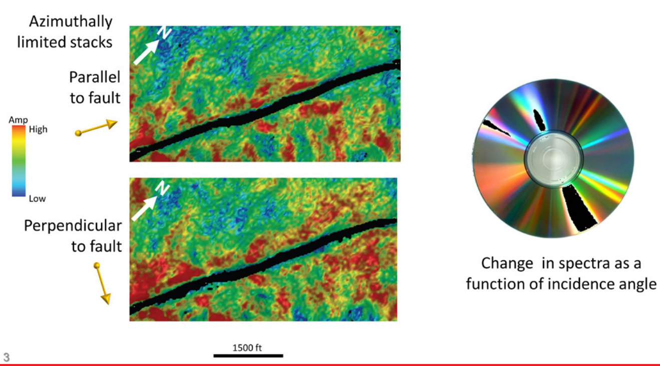

Figure 12: An example demonstrating azimuthally-limited seismic amplitude at (Top Left) azimuth 0–30° and at (Bottom Left) azimuth 90–120°, associated with a major northeast-trending fault in the fractured Barnett Shale in the Fort Worth Basin, Texas. Notice the amplitude response at azimuth 90–120° (perpendicular to the fault) is stronger than that at azimuth 0–30° (parallel to the fault), which is here interpreted to be physically related to textural roughness and texture anisotropy caused by faulting and fracturing. (After Gao, 2012)

image the data, subtract the perfectly good, stronger specular reflections, and somehow image the remaining, weaker diffractions (***Figure 13***).

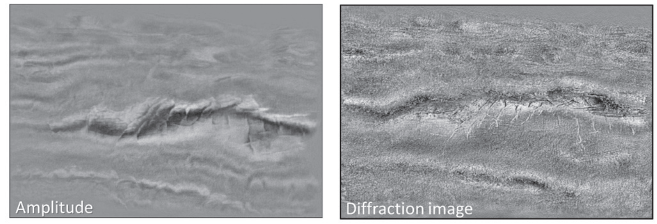

Figure 13: Seismic velocity analysis, statics, and other processing steps attempt to maximize the coherence of the specular reflections. Small errors in these parameters may result in misfocusing of the diffraction energy. One implementation of diffraction image begins with conventional seismic processing and imaging. The specular reflections are then filtered or otherwise enhanced and demigrated to remove the strong specular reflections in the seismic data. Several workers then subject this diffraction-rich data volume to a second pass of velocity analysis prior to migration. Whatever the workflow, the resulting diffraction image enhances edges associated with faults, joints, and lateral stratigraphic boundaries such as this image through an Eagle Ford Shale survey at 9000 ft depth. (Images courtesy of Z-terra. Seismic data courtesy of Seitel).

Next Up: ***Where will we be going? - Part 2 of 2***

References

Bahorich, M. S., and P. van Bemmel, 1994, Stratigraphic interpretation of seismic data on the workstation: 64th Annual International Meeting of the SEG, Expanded Abstracts, 481-484.

Bahorich, M. S., and S. L. Farmer, 1995, 3D seismic coherency for faults and stratigraphic features: The Leading Edge, 14, 1053-1058.

Balch, A. H. 1971, Color sonograms: A new dimension in seismic data interpretation, Geophysics, 36, 1074-1098.

Bellman, L., 2014, The evolution of interpretation: CSEG Symposium, Calgary.

Bueno, J. F., B. C. Zanardo Honório, , M. Chaves Kuroda, A. Campane Vidal, , and E. Pereira Leite, 2014, Structural and stratigraphic feature delineation and facies distribution using seismic attributes and well log analysis applied to a Brazilian carbonate field: Interpretation, B, SA83–SA92.

Chopra, S., and K. J. Marfurt, 2015, Is curvature overrated? It depends on the geology!: First Break, in press.

Gao, D., 2012, Implications of the Fresnel-zone texture for seismic amplitude interpretation: Geophysics, 77, O35-O44.

Guo, S., 2014, Seismic solutions for unconventional resource plays: Ph.D. dissertation, The University of Oklahoma.

Heritier, F. E., P. Lossel, and E. Wathe, 1979, Frigg Field; large submarine-fan trap in lower Eocene rocks of North Sea Viking graben: AAPG Bulletin,. 61, 1999-2020.

Kozlov, E. N. Brasky, and E. Korolev, 2004, Imaging scattering objects masked by specular reflections: 74th Annual International Meeting of the SEG, 1131-1134.

Lindseth, R. O., 1979, Synthetic sonic logs—a process for stratigraphic interpretation: Geophysics, 44 , 3-26.

Marfurt, K. J., 2015, Techniques and best practices in multiattribute display: Interpretation, 3, B1-B23.

Masaferro, J. L., R. Bourne, and J.-C. Jauffred, 2003, 3D seismic imaging of carbonate reservoirs and structures: The Leading Edge, 22, 18-25.

McArdle, N., D. Iacopini, M. A. Kunle-Dare, and G. S. Paton, 2014, The use of geologic expression workflows for basin scale reconnaissance: A case study from the Exmouth Subbasin, North Carnarvon Basin, northwestern Australia: Interpretation, 2, SA163–SA177.

Murray, G.H. Jr., 1968, Quantitative Fracture Study-Sanish Pool, McKenzie County, North Dakota: AAPG Bulletin, 52, 57-65.

Perez-Altamar, R., and K. J. Marfurt, 2014, Mineralogy-based brittleness prediction from surface seismic data: Application to the Barnett Shale, Interpretation, 2, T255-T271.

Rijks, E. J. H., and Jauffred, J. E. E. M., 1991, Attribute extraction: An important application in any 3-D seismic interpretation: The Leading Edge, 10, no. 9, 11-19.

Roberts, A., 2001, Curvature attributes and their application to 3D interpreted horizons. First Break, 19, 85-99.

Stephens, A., R. Meek, and P .Clarke, 2011, Mining Eagle Ford rock properties data from 3D seismic in south Texas using prestack inversion and neural net technology: Presented at the 17th Annual 3D Seismic Symposium, Rocky Mountain Association of Geologists.

Taner, M. T., F. Koehler, and R. E. Sheriff, 1979, Complex seismic trace analysis: Geophysics, 44, 1041-1063.

White, H. G. III, 2013, Fracturing of Mississippi Lime, Oklahoma: Experimental, seismic attribute, and image log analysis: M.S. Thesis, The University of Oklahoma

Zhao, T., V. Jayaram, K. J. Marfurt, and H. Zhou, 2014 Lithofacies classification in Barnett Shale using proximal support vector machines: 84th Annual International Meeting of the SEG, Expanded Abstracts, 1491-1495.

http://dx.doi.org/10.1190/segam2014-1644.1